HHS Public Access

Author manuscript

Nat Commun. Author manuscript; available in PMC 2016 June 01.

Published in final edited form as:

Nat Commun. ; 6: 7288. doi:10.1038/ncomms8288.

Coordination and Fine Motor Control Depends on Drosophila TRPγ

Bradley Akitake[1], **Qiuting Ren**[2], **Nina Boiko**[3], **Jinfei Ni**[1,2], **Takaaki Sokabe**[1], **James D. Stockand**[3], **Benjamin A. Eaton**[3], and **Craig Montell**[1,*]

[1]Neuroscience Research Institute and Department of Molecular, Cellular and Developmental Biology, University of California Santa Barbara, Santa Barbara, CA, 93106, USA

[2]Department of Biological Chemistry, The Johns Hopkins University School of Medicine, Baltimore, MD 21205, USA

[3]Department of Physiology, University of Texas Health Sciences Center, San Antonio, TX 78229, USA

Abstract

Motor coordination is broadly divided into gross and fine motor control, both of which depend on proprioceptive organs. However, the channels that function specifically in fine motor control are unknown. Here, we show that mutations in *trpγ* disrupt fine motor control while leaving gross motor proficiency intact. The mutants are unable to coordinate precise leg movements during walking, and are ineffective in traversing large gaps due to an inability in making subtle postural adaptations that are requisite for this task. TRPγ is expressed in proprioceptive organs, and is required in both neurons and glia for gap crossing. We expressed TRPγ *in vitro*, and found that its activity is promoted by membrane stretch. A mutation eliminating the Na^+/Ca^{2+} exchanger suppresses the gap crossing phenotype of *trpγ* flies. Our findings indicate that TRPγ contributes to fine motor control through mechanical activation in proprioceptive organs, thereby promoting Ca^{2+} influx, which is required for function.

Even the most basic tasks, such as acquiring food, locating safe places to rest, avoiding and defending against enemies, and mating requires motile animals to navigate through their environment by moving multiple body parts in a highly coordinated manner. To move fluidly, both vertebrate and invertebrate animals employ complex mechanosensory organs that are designed to gather and interpret feedback information about their movement in real-time through an array of specialized receptors and neural networks[1, 2]. These proprioceptive

*correspondence: phone, 805-893-3634, craig.montell@lifesci.ucsb.edu.

Author Contributions

C.M. and B.A. conceived and designed the experiments. B.A. and Q.R. generated the null mutant lines, transgenic fly lines, and antibodies. B.A. performed the behavioral experiments, microscopy and EMGs. N.B., J.D.S. and B.A.E. conducted patch-clamp experiments using hypoosmotic stimulations. B.A. and T.S. conducted patch-clamp experiments using pressure stimulations. Q.R. and J.N. performed and analyzed the actometer assays. C.M. and B.A. wrote the manuscript.

Competing Interest

The authors declare no competing financial interests.

sensory systems provide animals with continuously updated maps of their body positions that are critical for balance and locomotion.

Proprioception is mediated at the cellular level, by stretch-sensitive cells located in muscles, ligaments, and joints that are activated by mechanical forces[3, 4, 5]. In humans, damage to proprioceptive afferents results in a variety of movement disorders such as spasticity, impaired load sensitivity, and altered gait[6]. Proprioceptive dysfunction is also a clinical feature of diseases that affect the nervous system such as Parkinson's disease[5, 7, 8, 9, 10]

The worm, *C. elegans*, and the fruit fly, *Drosophila melanogaster*, have served as animal models for characterizing proprioception. Both of these organisms display highly stereotypic locomotion[11, 12, 13, 14, 15], which has facilitated the identification of neurons and ion channels that function in proprioception[14, 15, 16, 17, 18]. In flies, proprioceptive neurons are located in specialized sensory structures: mechanosensory bristles, campaniform sensilla, and chordotonal organs[19]. Several invertebrate members of the Transient Receptor Potential (TRP) family of cation channels localize to proprioceptive cells and contribute to sensing bodily movements during locomotion. These include the *C. elegans* and Drosophila TRPN channels, TRP-4 and NOMPC, respectively, which are required for worms and fly larvae to make the gross postural changes during locomotion[14, 17, 20]. Most *nompC* mutant animals die during the pupal stage[20, 21]. The few mutant animals that survive to adulthood exhibit severe locomotion defects and uncoordinated movement of body parts, indicative of defects in gross motor control[17]. Mutations disrupting the Drosophila TRPV channels, Inactive (Iav) and Nanchung (Nan) also result in severe locomotor defects[11, 22, 23, 24].

A key question is whether there exist ion channels that specifically function in fine motor control. In flies, a defect in fine motor control would not eliminate behaviors that rely principally on gross movements of the body and appendages, such as negative geotaxis, or crossing small gaps. However, loss of fine motor control would be expected to impair performance when the flies are faced with highly challenging tasks, such as traversing wide gaps, which rely on coordinating a repertoire of fine movements, including subtle changes in body angles and leg positions[11, 12].

The Drosophila genome encodes 13 TRPs, 12 of which have been subjected to genetic analyses[16, 25]. The recurring theme is that these channels are essential for sensory physiology. However, the function of one Drosophila TRP channel, TRPγ, is not known. TRPγ is a TRPC channel[26], and is most related to the founding TRP channel[27]. In this study we demonstrate that TRPγ is localized to neurons and glia that comprise the femoral chordotonal organs. We generated *trpγ* null mutant flies and found that they were distinct from the *nan* and *iav* mutants in that they displayed much greater levels of negative geotaxis and were proficient in crossing small gaps. However, once the gaps become challenging but were still surmountable for most wild-type flies, the *trpγ* mutants were unable to make the fine postural adaptations required for negotiating the gaps. Thus, this phenotype sharply contrasted with the loss of other TRP channels that impact on proprioception, as TRPγ was uniquely required to promote highly coordinated motor control. These data demonstrate that fine motor control is not mediated exclusively through the same repertoire of cation channels that function in gross motor control.

Results

Expression of the *trpγ* reporter in proprioceptive organs

To obtain clues as to the roles of *trpγ*, we generated a gene reporter to examine its expression pattern. We used homologous recombination[28] to insert the yeast *GAL4* gene at the site of the ATG. To simultaneously generate a mutant allele, we deleted 547 base pairs extending 3′ from the start codon with the *GAL4* gene (*trpγ*^{G4}; Fig. 1a, b). Using *trpγ*^{G4}/+ in conjunction with *UAS-DsRed*, we found that the *trpγ* reporter was expressed prominently in femoral chordotonal organs (Fig. 1c, d), which are responsible for sensing stretch and the position of the fly legs[29]. The reporter also labeled neurons in macrochaetes (mechanosensory bristles)[20] on the dorsal thorax and legs (Fig. 1e, f).

TRPγ was required for the rapid righting reflex

The expression of the *trpγ* reporter in proprioceptive organs raised the possibility that TRPγ was required for coordination or locomotor activity. To examine the role of TRPγ we characterized *trpγ*^{G4} animals, as well as a second mutant allele, *trpγ*^{1}, which we generated by homologous recombination (Supplementary Fig. 1a, b). The *trpγ*^{1} mutation removed 180 base pairs that encoded the C-terminal portion of the 6th transmembrane domain as well as the highly conserved TRP box (EWKFAR)[30]. Both *trpγ*^{1} and *trpγ*^{G4} were homozygous viable and fertile.

To assay overall locomotor activity, we used an actometer (Drosophila Activity Monitoring System) and found that the mutant flies showed a decrease in overall activity (Supplementary Fig. 2a). Both *trpγ*^{1} and *trpγ*^{G4} mutant flies also displayed a small but significant negative geotaxis defect, which we assayed by gently tapping down the flies in a graduated cylinder (Supplementary Fig. 2b). However, in contrast to the severe reduction in climbing indexes exhibited by flies missing either of the TRPV channels, Nan (*nan*^{36a}) and Iav (*iav*^{1}; originally called *hypo*^{B})[22, 23], the *trpγ* mutant flies showed only mild impairments in this behavior (Supplementary Fig. 2b).

Wild-type flies have a rapid righting reflex, which depends on using alternating legs to push against the ground, thereby enabling them to turn over. Because the speed of this reflex requires coordinated movements of the legs, we wondered whether the turnover behavior was impaired in the mutant animals. After taping down flies in a cylinder, wild-type flies righted themselves in slightly more than one second (1.19 ± 0.24 sec, mean ±SEM; Fig. 2a; Supplementary Fig. 2c and Supplementary Movie 1). In contrast, *trpγ*^{1} and *trpγ*^{G4} animals required four times longer to complete the righting reflex (4.76 ± 2.39 and 3.72 ± 1.81 sec, respectively; Fig. 2a; Supplementary Fig. 2c). This delay in righting did not appear to be due to defects in sensing the supine position, as the mutant flies were actively engaged in righting attempts immediately after the tap down, similar to wild-type. We rescued this phenotype with either a genomic transgene (*gtrpγ*) or with a *UAS-trpγ* transgene, using the *GAL4* inserted into *trpγ*^{G4} (1.11 ± 0.45 and 1.76 ± 0.68 sec, respectively; Fig. 2a).

Mutation of *trpγ* impaired leg coordination during walking

The defect in the righting reflex suggested that leg movement coordination might be compromised in the *trpγ* mutants. To assess this question quantitatively, we performed a video analysis of flies walking over a catwalk. We mounted the camera orthogonally to the catwalk at the level of the walking surface, and recorded at an increased speed (200–250 frames per second) as the flies traversed the platform (Fig. 2b). We tracked the movements of the three legs facing the camera or the set facing away. From this perspective, the leg movements of wild-type animals were highly coordinated such that all three legs contacted the catwalk on nearly the same points (Fig. 2c and Supplementary Movie 2), due to the flies alternating tripod gait[11, 13]. From these leg tracks we measured the walking speed, the inter-step distances for the front, middle, and hind legs, as well as the dispersion of the footprint clusters (Fig. 2d–f).

We found that loss of *trpγ* reduced the speed and precision of movements during walking (Supplementary Movie 3). The *trpγ* mutant animals showed a 28–33% decrease in forward walking speed (wild-type, 22.7 ±1.5 mm/sec, mean ±SEM; $trp\gamma^{1}$, 15.2 ±0.2 mm/sec; $trp\gamma^{G4}$, 16.3 ±0.4 mm/sec; Fig. 2d) accompanied by a 19–25% shorter average step length (wild-type, 2.28 ±0.08 mm, mean ±SEM; $trp\gamma^{1}$, 1.70 ±0.15 mm; $trp\gamma^{G4}$, 1.84 ±0.14 mm; Fig. 2f). Of greatest significance from the perspective of coordination, the footprint cluster dispersions of $trp\gamma^{1}$ and $trp\gamma^{G4}$ were increased ~60% (wild-type, 0.23 ±0.04 mm, mean ±SEM; $trp\gamma^{1}$, 0.39 ±0.07 mm; $trp\gamma^{G4}$, 0.36 ±0.05 mm; Fig. 2e). The iav^{1} and nan^{36a} mutants displayed similar footprint cluster dispersion deficits (iav^{1}, 0.39 ±0.08 mm; nan^{36a}, 0.36 ±0.06 mm; Fig. 2e). We did not analyze *nompC* mutants since too few of these animals survived to adulthood. Introduction of the wild-type *trpγ* genomic transgene (*gtrpγ*) rescued the walking defects displayed by *trpγ* mutants (Fig. 2d–f).

trpγ mutants showed defects in traversing large gaps

To further evaluate leg coordination in $trp\gamma^{1}$ and $trp\gamma^{G4}$, we increased the difficulty of the locomotor task by adding gaps of varying widths to the catwalk. The number of approaches per attempt increased with the gap width (Fig. 3a, b). If the gaps were relatively short (2.5 mm), most approaches by wild-type flies were followed by an attempt at a gap crossing (1.3 ±0.4 approaches/attempt, mean ±SEM; Fig. 3b). If the gap width was increased to 4.0 mm, then the number of approaches per attempt nearly doubled (2.4 ±0.1 approaches/attempt; Fig. 3b).

The increase in approaches per attempt was inversely proportional to success of the wild-type flies to traverse the gap. At a gap width of 2.5 mm, 93 ±2.6% of the attempts (mean ±SEM) were successful (Fig. 3c, d). A majority of crossing attempts were still successful at 3.5 mm (59.2 ±5.3%; Fig. 3c–e) a gap width ~1.5 times the flies' average body length of 2.26 ±0.04 mm (mean ±SEM, Fig. 3a, b and Supplementary Table 1). A minority of crossing attempts was successful at the 3.75 mm gap (16.0 ±3.4%; Fig. 3d), and very few flies were able to surmount a 4.0 mm divide (2.0 ±1.3%; Fig. 3d).

The $trp\gamma^{1}$ and $trp\gamma^{G4}$ animals initiated gap crossing with a frequency similar to wild-type (Fig. 3b), but were impaired in traversing larger gaps (Fig. 3d). At distances of ≤3.0 mm,

trpγ mutant animals were equally successful at negotiating gaps as wild-type flies (Fig. 3d). However, their success was reduced significantly as the sizes of the openings increased. The differences between wild-type and the mutants were most pronounced at the 3.5 mm gap width. Wild-type animals crossed this gap more than half of the time. However, the 3.5 mm opening was nearly insurmountable for the *trpγ* mutants ($trp\gamma^{1}$, 6.0 ±3.4%; $trp\gamma^{G4}$, 8.4 ±2.7%; Fig. 3d, e). This ineffectiveness was not due to a shorter body length ($trp\gamma^{1}$, 2.29 ±0.02 mm; $trp\gamma^{G4}$, 2.17 ±0.03 mm; Fig. 4a, b and Supplementary Table 1). The gap crossing impairment reflected a requirement for the *trpγ* gene, since we observed the same phenotype in both mutant alleles, in trans-heterozygous flies, and when we placed the $trp\gamma^{1}$ mutation *in trans* with a deficiency uncovering the mutation (Fig. 3e). We restored normal crossing ability with a wild-type *gtrpγ* genomic transgene ($trp\gamma^{1}$;*gtrpγ*, 50.5 ±3.8%; Fig. 3e). The *trpγ* phenotype was distinct from iav^{1} and nan^{36a} mutants, which failed in their attempts at surmounting much shorter gap distances (Fig. 3d).

Impairments in postural adaptations to extend reach

Gap crossing is a highly stereotyped behavior that flies perform by making progressive postural adjustments in their horizontal body distance, body angle, and front leg reach (Fig. 4a and Supplementary Movie 4)[12]. To assay the horizontal body distance and postural adaptations in body angle, we tracked both the head and posterior positions of the flies during crossings over a 3.5 mm gap. As soon as wild-type flies extended their bodies over a gap to attempt a crossing, they began to perform leg over head (LOH) strokes (Fig. 4a and Supplementary Movie 4). With each subsequent LOH stroke the flies adjusted their posture aiming to maximize their reach across the gap. We compared the body positions and angles at the initiation of each crossing (first LOH stroke) and at the end of each crossing, just before the front legs contacted the opposite side, or when the flies gave up and turned back (last LOH stroke). Wild-type flies increased their horizontal body positions by 0.23 ±0.05 mm (mean ±SEM, Fig. 4c) and flattened their body angles towards horizontal by 13.6 ±2.3° (mean ±SEM, Fig. 4d). To assay the front leg reach postural adaptation, we tracked the positions of the flies' front legs relative to the head during crossings. Wild-type flies extended their front legs during gap crossing, and improved their reach by 0.26 ±0.04 mm (mean ±SEM, Fig. 4e).

We found that the *trpγ* mutant animals were unable to optimally perform postural adjustments while attempting to cross a 3.5 mm gap (Supplementary Movie 5). The $trp\gamma^{1}$ and $trp\gamma^{G4}$ flies were able to increase their horizontal body distances over the gap (0.42 ±0.06 and 0.39 ±0.11 mm, respectively; Fig. 4c). However, in contrast to wild-type, the body angles of the *trpγ* mutants remained near their starting angles and did not increase throughout their crossing attempts ($trp\gamma^{1}$, −1.9 ±2.8° and $trp\gamma^{G4}$, −1.5 ±3.5°; Fig. 4d). In addition, the *trpγ* mutant flies did not fully extend their front legs ($trp\gamma^{1}$, 0.09 ±0.03 mm; $trp\gamma^{G4}$, 0.13 ±0.06 mm; Fig. 4e). After we introduced a wild-type *trpγ* transgene (*gtrpγ*), in the $trp\gamma^{1}$ background, all of the postural adjustments were similar to wild-type (body distance, 0.31 ±0.08 mm; body angle, 10.6 ±1.5°; front leg reach, 0.23 ±0.04 mm; Fig. 4c–e).

With each LOH stroke wild-type flies update their body posture as they attempt to bridge a gap. The total number of LOH strokes is tightly regulated in wild-type flies as this is thought to reduce the expenditure of energy wasted during attempts to traverse insurmountable gaps[12]. Wild-type flies performed 3.6 ±0.4 LOH strokes during a 3.5 mm crossing (mean ±SEM, Fig. 4f). The $trp\gamma^{1}$ and $trp\gamma^{G4}$ mutants performed 3.4 to 4.0 times more LOH strokes, and the variation in number was much greater than was typical of wild-type flies (12.2 ±2.0 and 14.5 ±2.5 strokes, respectively; Fig. 4f). Some of the $trp\gamma$ mutant flies produced strikingly large numbers of LOH strokes such that the maximum number was up to 10 times greater than wild-type (Fig. 4f). Introduction of $gtrp\gamma$ in $trp\gamma^{1}$ animals restored a level of LOH strokes that was similar to wild-type (4.82 ±0.72 strokes; Fig. 4f).

Cellular localization of TRPγ in the femoral chordotonal organs

The femoral chordotonal organ is located in the proximal part of each femoral leg segment (Fig. 5a), and is comprised of three large groups of aligned scolopidia (Fig. 5b). Each group contains between 10 to 35 scolopidia (Fig. 5c)[31].

A scolopidium is the fundamental mechanosensitive unit of the insect chordotonal organ and consists of four cell types: 1) two bipolar neurons (N), 2) one glial cell (scolopale cell; SC), 3) one cap cell (CC), and 4) one ligament cell (LC) (Fig. 5d)[19]. The dendrites of the bipolar neurons have two distinct regions demarcated by a ciliary transition root (ctr, yellow arrow; Fig. 5d). In the proximal scolopidial region (PSR) the dendrites are larger in diameter than in the distal scolopidial region (DSR) (red and blue dashed lines, respectively; Fig. 5d). The scolopale cell encloses a wide extracellular space (scolopidial space; ss). The thin sensory cilia (ci), which comprise the distal region of the dendrites, extend through the scolopidial space and terminate at the cap cell. The cap cell mechanically couples the scolopidium to either the epicuticular surface or femoral muscle membranes via a ligament cell (Fig. 5d).

The distinctive morphologies and positions of the cells within a scolopidium allowed us to identify the cell types labeled by the $trp\gamma$ reporters. The neuronal-specific marker, *elav-GAL4*, labeled the neuronal cell bodies (ncb+) in the PSR (blue dashed line) (Fig. 5e). This reporter also stained the ciliary transition roots (ctr, yellow arrow) and the sensory cilia (ci+, red dashed line), but not the scolopale cells (SC−) (Fig. 5e lower panel). The labeling of the sensory cilia was weak due to the narrow diameter of these dendrites. To specifically mark the scolopale cells, we used the *nompA-GAL4*[32, 33] (Fig. 5f; SC+, blue dashed line). The SC + staining was considerably wider in diameter than either the proximal or distal dendritic signals, consistent with the morphology of scolopale cells.

We found that the $trp\gamma$ reporter ($trp\gamma^{G4}$/+) stained both neurons and glia (scolopale cells) in the FCO. Consistent with neuronal expression, the $trp\gamma$ *GAL4* stained the neuronal cell bodies (ncb+), and the proximal dendritic projections in the PSR (red dashed line) (Fig. 5g). The reporter also marked the ciliary transition roots (ctr, yellow arrow) and cells in the DSR (blue dashed line) (Fig. 5g). The morphology of these distal cells was consistent with expression in scolopale cells (SC+; Fig. 5g, upper and lower panel).

To confirm that the $trp\gamma$ reporter reflected the *bona fide* expression pattern, and to determine the subcellular localization of the TRPγ protein, we generated TRPγ antibodies (α–TRPγ).

The antibody accessibility was poor in whole mount leg samples and standard fixation methods followed by frozen or resin embedded sectioning resulted in damaged FCO morphology. Therefore, to better preserve the FCO ultrastructure, we subjected whole legs to high pressure freezing followed by low temperature fixation and embedding though automated freeze substitution[34]. We immunostained sections, and found that the α–TRPγ antibodies labeled the proximal dendrites and neuronal cell bodies (ncb+) in the PSR (red dashed line) and the scolopale cells (SC+) surrounding the scolopidial spaces in the DSR (blue dashed line) (Fig. 5h). Labeling was strongest towards the distal ends of the scolopale cells, while the signal in the neuron cell bodies was more diffuse (ncb+). We also detected weak α–TRPγ signals in the extremely thin sensory cilia in the scolopidial spaces (white asterisks, placed at proximal end of visible cilia signal) (Fig. 5i). Neither of two neuronal-specific antibodies (anti-ELAV or anti-22C10) stained these sections, precluding double-labeling experiments. Nevertheless, the α–TRPγ signal appeared to be specific since we did not detect staining in the *trpγ*^{1} mutant (Fig. 5j).

Loss of TRPγ disrupted the resistance reflex

To assess the functional consequences due to loss of TRPγ, we performed extracellular myogram (EMG) recordings and measured the resistance reflex in muscle cells that depended on functional neurons in femoral chordotonal organs (FCOs)[35, 36, 37, 38]. We placed a sharp borosilicate electrode under the cuticle of the femur and recorded excitatory responses from the tibial extensor muscles in response to rhythmic movement of the tibia about the femoral joint. A 2 Hz movement of the wild-type tibia elicited robust firing of the slow extensor motor neurons (Fig. 6a, c; 107.2 ±11.5 spikes/360° cycle of movement, mean ±SEM). We found that these motor neurons were silent in the absence of flexion. However, *trpγ* mutant animals displayed ~40–58% reductions in the frequencies of action potentials in response to tibia deflections (Fig. 6b, c; *trpγ*^{1}, 64.8 ±8.6 spikes/cycle; *trpγ*^{G4}, 64.4 ±7.5 spikes/cycle; *trpγ*^{1}/*trpγ*^{G4}, 45.8 ±8.3 spikes/cycle). While the frequencies of action potentials were decreased, the mutant animals retained synchronous firing patterns. We restored a wild-type level of action potentials with a genomic transgene (Fig. 6c; *gtrpγ*; 105.0 ±13.6 spikes/cycle), or by expressing a *trpγ* transgene (*UAS-trpγ*) under control of the *trpγ* promoter (*GAL4* knocked into *trpγ* locus) (Fig. 6c; *trpγ*^{G4}; 107.2 ±13.0 spikes/cycle).

Cell-type requirement for *trpγ* in chordotonal organs

To determine the cell type specific requirement for TRPγ for the mechanically evoked response, we recorded EMGs from *trpγ* null animals after restoring *trpγ* expression (*UAS-trpγ*) only in chordotonal neurons (*iav-GAL4*) or in scolopale cells (*nompA-GAL4*). We found that expression of *trpγ* in chordotonal neurons but not scolopale cells rescued the *trpγ* EMG phenotype (Fig. 6c; 91.6 ±7.6 spikes/cycle and 63.8 ±6.2 spikes/cycle, respectively).

To investigate the cellular requirement for TRPγ for successful gap crossing, we performed RNAi knockdown and *UAS-trpγ* rescue experiments. We then assayed for proficiency at traversing 3.5 mm gaps. The *UAS-trpγ* RNAi was effective, since we phenocopied the gap-crossing deficit using the *trpγ-GAL4* (compare *trpγ*^{G4}/+ with and without the *UAS-trpγ* RNAi; Fig. 7a). We recapitulated the *trpγ* mutant phenotype using all three neuronal drivers tested: *elav-GAL4*, *nanchung* (*nan*)-*GAL4* or *inactive* (*iav*)-*GAL4* (Fig. 7a). Knockdown of

UAS-trpγ in scolopale cells using the *nompA-Gal4* impaired gap crossing, through not to the same extent as the neuronal *GAL4* drivers (Fig. 7a). Knockdown of *trpγ* with a cap cell specific *GAL4*, *pyrexia (pyx)-GAL4*[39], did not affect gap crossing (Fig. 7a). We also tested the *atonal (ato)-GAL4*, which is expressed in both neurons and scolopale cells of the chordotonal Johnston's organ[33]. However, the *ato-GAL4* did not cause any effect in the RNAi experiments (Fig. 7a), or drive detectable *UAS-GFP* expression in the FCO.

We also tested for rescue of the *trpγ* gap crossing defects with a wild-type *trpγ* transgene. Introduction of the *UAS-trpγ* transgene in $trp\gamma^{G4}/trp\gamma^{1}$ flies fully rescued the mutant phenotype (Fig. 7b). The rescue required the $trp\gamma^{G4}$ driver since the *UAS-trpγ* transgenes did not restore gap crossing performance in $trp\gamma^{1}$ flies, which did not include a *GAL4* knocked into the *trpγ* gene (Fig. 7b). We found a significant rescue of the mutant phenotype using either neuronal *GAL4* tested (*elav-Gal4* and *iav-Gal4*; Fig. 7b). We partially rescued the gap-crossing phenotype by driving *UAS-trpγ* expression only in scolopale cells with the *nompA-GAL4* (Fig. 7b).

Consistent with a contribution of *trpγ* to scolopale function, we found that the vacuolar volume of the scolopale cells was reduced in $trp\gamma^{1}$ (Supplementary Fig. 3a, b). Except for the reduced size of the scolopale cells, we did not detect other changes in the ultrastructure of the mutant scolopidia. The scolopale rods, scolopale spaces, the neuron cell bodies, dendrites, and the dendritic connection to the cap cell all appeared intact and comparable to wild-type (Supplementary Fig 3a, c).

Suppression of the *trpγ* phenotype by mutation of CalX

Because TRPγ is a Ca^{2+}-permeable channel, the loss of the TRPγ-dependent Ca^{2+} influx might underlie the proprioceptive defects. To address this model, we applied an approach that we used previously to show that the retinal degeneration in fly photoreceptor cells that resulted from loss of the TRP channel, was due to a decrease in light-dependent Ca^{2+} influx. Specifically, we showed that loss of either TRP or the only Na^{+}/Ca^{2+} exchanger (CalX) expressed in flies caused retinal degeneration[40, 41]. However, the retinal degeneration was much less severe in the double mutant[40, 41]. Therefore, we wondered whether we could suppress the $trp\gamma^{1}$ phenotype by introducing the $calx^{B}$ mutation, since we found that CalX antibodies (α–CalX)[41] stained neurons and scolopale cells of the wild-type FCO (white dashed outline; Fig. 7c). The specific labeling in wild-type was absent in the $calx^{B}$ FCO, although there was some background staining, especially of the cuticle (cu) (white dashed outline; Fig. 7c). In behavioral assays, loss of CalX alone ($calx^{B}$), caused a gap crossing deficit, similar to that displayed by *trpγ* mutant flies (Fig. 7d; wild-type, 63.5 ±4.2%, mean ±SEM; $trp\gamma^{1}$, 11.6 ±5.9%; $calx^{B}$, 12.2 ±8.8%). However, when we introduced the $calx^{B}$ mutation in a *trpγ* mutant background, the defect in gap crossing ability was suppressed significantly, as it was less severe than that exhibited by either single mutant alone (Fig. 7d; $trp\gamma^{1}$;$calx^{B}$, 42.8 ±3.3%).

TRPγ was activated by membrane stretch *in vitro*

The contribution of TRPγ to fine motor control raises the possibility that it is a mechanically-sensitive channel (MSC). The activities of MSCs are typically enhanced by

membrane stretch[42]. To investigate whether TRPγ might be sensitive to membrane stretch, we expressed TRPγ in HEK293 cells and performed whole cell recordings. We first tested whether macroscopic TRPγ currents were enhanced by bathing the cells in hypotonic (210 mOsm) media. When we performed the recordings under isotonic (300 mOsm) conditions, there was a constitutive, strongly outwardly-rectifying conductance (Fig. 8a, b), consistent with previous findings[26, 43]. Upon exchanging the external media with a hypoosmotic (210 mOsm) bath solution, the current increased 3-fold (Fig. 8a–d). We blocked this activity with Gd^{3+} (Fig. 8a), an inhibitor of TRPγ[26, 43]. The current began to increase within 30 seconds, after switching from 300 to 210 mOsm media, and peaked between ~1 to 4 minutes, depending on the experiments (closed squares, Fig. 8b). We did not detect a constitutive or hypoosmotic-induced current in mock-transfected cells (open circles, Fig. 8b). Many TRPC channels are activated through phospholipase C (PLC) signaling cascades. However, addition of a PLC blocker (U73122) did not affect the hypoosmotic induced TRPγ currents (Fig. 8e), suggesting that the hypotonicity impacted on TRPγ activation through membrane stretch rather than stimulation of PLC signaling.

To test if TRPγ could be activated directly by membrane stretch, we applied positive pressure to HEK293 cells in the whole cell configuration through the recording pipet (Fig. 8f)[44]. We found that repeated pressure stimulations between +30 to 300 mmHg, starting from a resting pressure of −10 mmHg, enhanced the current in TRPγ expressing cells (Fig. 8g–i). Moreover, hypoosmotic stimuli or mechanical pressure steps enhanced the conductance in every patched cell that displayed constitutive TRPγ activity (Fig. 8c, i).

Discussion

In humans, motor control is categorized into two major types: gross motor skills, required for large body movements such as sitting upright or waving an arm, and fine motor skills, necessary for small precise movements such as picking up and manipulating objects[45]. In Drosophila, gross motor coordination is essential for the large rhythmic movements of the body and limbs during general locomotion (walking), while fine motor coordination is critical for making small changes in the angles and positions of the body and appendages to complete difficult tasks, such as righting or navigating gaps in a terrain.

Three Drosophila TRP channels are expressed in proprioceptive organs (Iav, Nan and NOMPC) and elimination of any of these proteins have severe effects on locomotion and gravity sensation[17, 22, 23, 24]. Due to the major locomotor deficits resulting from the loss of any of these channels, fine motor control is also profoundly affected.

Prior to the current study, it was unclear whether there existed cation channels that contribute exclusively to highly coordinated movements of the body and appendages. In principle, it was possible that the two types of motor coordination depended on the same repertoire of channels (e.g. Iav and Nan), and that null mutations would strongly impair all types of coordinated movements, while hypomorphic mutations would affect fine motor control only.

We found that TRPγ was required exclusively for fine motor behaviors. In high-frame rate video analysis, both wild-type and *trpγ* flies traversed the catwalk at a relatively fixed maximum speed, though the *trpγ* mutants walked more slowly and displayed decreased precision in their leg placements. However, the *trpγ* mutants used consistently shortened steps, which differed from the abnormally long and highly variable step lengths exhibited by *nan* mutants[11].

The impairments in fine motor control exhibited by *trpγ* flies compromised their ability to cross challenging gap sizes. While the mutant animals negotiated gaps of up to 3.0 mm as well as wild-type, they were ineffective in traversing larger gaps. This defect was not due to smaller flies, since the lengths of the *trpγ* bodies were similar to wild-type animals. We propose that the impairment in gap crossing arises from the inability of the mutants to precisely sense their body position and make the fine postural adjustments required to complete the task. Indeed, the *trpγ* flies were unable to increase their body angles towards the horizontal position, even as they made successive leg-over-head sweeps. Consequently, they could not fully extend the reach of their front legs to bridge the gap. In sharp contrast, *nan* and *iav* mutants were not able to effectively cross even short gaps that virtually all *trpγ* and wild-type flies were able to negotiate.

The majority of work on Drosophila proprioceptive organs has focused on the contribution of the mechanosensory neurons to motor control[17, 20, 22, 23] Unexpectedly, we found that TRPγ was expressed and functioned in both neurons and in glial support cells, called scolopale cells. However, the requirement for TRPγ in neurons appeared to be more significant. RNAi knockdown of *trpγ* in neurons induced a gap-crossing deficit nearly as severe as the null mutations, while RNAi knockdown of *trpγ* in scolopale cells, caused a more modest effect. Moreover, we rescued the gap crossing impairment exhibited by *trpγ* to a greater extent after re-introducing the wild-type transgene in neurons than in scolopale cells. When we assayed the effects of the *trpγ* mutation on the leg motor circuit, using EMGs, we rescued the deficit in sensitivity only after expressing the wild-type transgene in neurons. Nevertheless, TRPγ has a dual role in both neurons and scolopale cells, and this is an additional feature that distinguishes TRPγ from TRPs that function in gross motor control.

In neurons, the spatial distribution of TRPγ is different from that of Iav, Nan, and NOMPC, consistent with the distinct roles of these channels in promoting fine and gross motor control, respectively. In contrast to the cilia-restricted localizations of Iav, Nan, and NOMPC[22, 46], we detected TRPγ throughout the neuronal cell bodies and dendrites.

We propose that TRPγ functions in chordotonal neurons to sense joint movements needed for fine motor control. In support of this proposal, TRPγ was activated directly by membrane stretch *in vitro*, and expressed in the dendrites. Furthermore, the TRPγ-dependent Ca^{2+}-influx contributes to function, since we suppressed the severity of the behavioral phenotype by eliminating the Na^{+}/Ca^{2+}-exchanger, CalX.

An additional question concerns the potential role of TRPγ in the scolopale cells. We found that the extensive vacuole network of the mutant scolopale cells in the FCO was reduced in

size compared to wild-type. Various mechanosensors contribute to maintaining vacuolar structures in cells[47, 48] and growing evidence suggests that TRP channels play critical roles in regulating cell size and shape[49]. This raises the possibility that TRPγ plays a similar role in these support cells, which in turn helps maintain the structural stability of the mechanosensory organs.

In summary, we employed high-frame rate video microscopy of fly locomotive behaviors to identify a requirement for a mechanosensitive TRP channel, TRPγ, for fine motor control. The demonstration that a Drosophila channel functions specifically to promote precise body movements raises the question as to whether there exist mechanosensitive Ca^{2+}-permeable channels in mammals that are uniquely required for fine motor control.

Methods

Fly stocks

All fly stocks used were maintained under standard laboratory conditions under a 12 hr light/12 hr dark cycle at 25°C. The control flies were Canton S flies, which we backcrossed for 10 generations to w^{1118}. We selected w^{+} progeny after each cross, to create the w^{CS} control flies. The *pyrexia-Gal4*, *nompA-Gal4*, and *atonal-Gal4* lines were provided by D. Eberl[33, 39]. The *UAS-trpγ* RNAi line was from the Vienna Drosophila Resource Center (transformant ID 107656). Df(2L)ED1109, *UAS-dsRed*, *UAS-mCD8::GFP*, *UAS-2xeGFP*, *elav-Gal4*, *iav-Gal4*, *nan-Gal4*, *nompC-Gal4*, iav^{1}, nan^{36a}, trp^{343}, and $trpl^{MB03075}$ were from the Bloomington Stock Center (Bloomington, IN). We described the $calx^{B}$ mutant previously[41].

Generation of $trp\gamma^{1}$ and $trp\gamma^{G4}$ by homologous recombination

We generated the $trp\gamma^{1}$ and $trp\gamma^{G4}$ mutants by ends-out homologous recombination[28]. To create $trp\gamma^{1}$, we deleted 180 nucleotides, encoding amino acids 607 to 667, and introduced the *white* gene at the site of the deletion. To generate $trp\gamma^{G4}$, we replaced 547 nucleotides that including the first two ATGs at the translation start site of *trpγ*, with a *GAL4* gene, which was flanked by the *white* gene.

To generate the pw35-$trp\gamma^{1}$ construct, we amplified 3.38 and 3.04 kb *trpγ* genomic fragments by PCR and subcloned them into the NotI site and the BamHI sites, respectively, of the pw35 vector[28]. The primers for generating the 3.38 kb fragment were: 5′-ATTTGCGGCCGCATCAACTTATTTCGGTGGGATACTTAC-3′ and 5′-ATTTGCGGCCGCACTTATGTAGTATGCGATTCGATTATTG-3′. The primers for PCRing the 3.04 kb fragment were 5′-GAAGATCTAAGAGGGTTTGTGTGGTTTCGAATAAAC-3′ and 5′-GAAGATCTTTCGCTTTGTTGGCTTGCATGTCTTTAGT-3′.

To generate pw35*Gal4-trpγ*^{G4}, we PCR amplified 3.42 and 2.98 kb *trpγ* genomic fragments, which we inserted between the BamHI/Acc65I sites and the NotI/SacII sites of the pw35*GAL4* vector, respectively[50]. The primers for amplifying the 3.42 kb fragment were: 5′-CGGGTACCTGCTGTGACGCTAAGGGATTAATAT-3′ and 5′-CGGGATCCTTTCTTTCGGTGTATTTCTCTGTA-3′. The primers for amplifying the 2.98

kb fragment were 5′-TCCCCGCGGTATTCCTGCTGTGGCGAGTTCTGCGCAT-3′ and 5′-ATTTGCGGCCGCCATGATGTGCGATGTGGCTGTGATGA-3′.

We introduced pw35-*trpγ*^{1} and pw35*Gal4-trpγ*^{G4} into *w*^{1118} flies by germline transformation. We generated homologous recombinants as described[28], and verified the mutations by PCR. We backcrossed *trpγ*^{1} and *trpγ*^{G4} for 10 generations to the *w*^{1118} background before conducting the behavioral analyses.

Generation of *UAS-trpγ* and *gtrpγ* transgenic lines

To generate *UAS-trpγ* flies, we PCR amplified the *trpγ* coding sequence from *w*^{1118} genomic DNA, which we subcloned between the NotI and the XbaI sites of pUAST[51]. We introduced pUAST-*trpγ* DNA into *w*^{1118} embryos via germline transformation (BestGene Inc., Chino Hills, CA), and recovered transformant lines with insertions in chromosome 2 and 3.

To generate the *trpγ* genomic transgene (*gtrpγ*), we used P[acman] BAC CH322-162M11[52], which covers the entire *trpγ* genomic region and truncates the 5′ and 3′ genes. We inserted P[acman] BAC CH322-162M11 by ϕC31-mediated transgenesis (Rainbow Transgenic Flies Inc., Camarillo, CA) into the VK00033 attP site on chromosome 3L (Bloomington stock #24871)[52, 53].

TRPγ antibodies

A TRPγ peptide (amino acids 1065–1085) was injected into rabbits to raise polyclonal antibodies (Covance Inc.). This sequence was unique among Drosophila proteins. We affinity purified the TRPγ antibodies (α–TRPγ) from whole serum using the synthesized peptide immobilized on an Affi-Gel 10 (Bio-Rad) column.

High pressure freezing and electron microscopy

We dissected Drosophila legs from 3–5 day-old male flies, and transferred them to yeast paste containing 10% methanol, or hexadecene, which served as a cryoprotectant[54]. The samples were then freeze substituted in a fixing cocktail containing 2% osmium and 0.2% uranyl acetate in acetone and 5% water for better preservation of membranes[55]. We performed the freeze substitution in a Leica EM AFS 2/FSP with a modified schedule (correspondence Rick Fetter, Janelia Farms HHMI). We incubated the samples at −90 °C for 72 hrs, brought them to −25 °C with a slope of 5 °C/hr, and then held them at −25 °C for 17 hrs to increase membrane contrast[56]. Samples were then sloped 5 °C/hr to 4 °C and held there for further processing. After three acetone rinses, we gradually infiltrated the samples at 25 °C with a mixture of Eponate 12 and Spurr's resin (1:1, Ted Pella) with acetone, 25% for 2 hrs, 50% for 2 hrs, and 75% overnight. After three exchanges with 100% resin, we cured the samples at 60°C for two days.

We oriented the blocks and cut longitudinal and cross sections through the femoral chordotonal organ on a Reichert Ultracut E with a Diatome Diamond knife. 60 nm sections were picked up on formvar coated 1 × 2 mm copper slot grids and stained with 2% uranyl acetate and 0.3% lead citrate. Grids were viewed on a Phillips CM 120 transmission EM

operating at 80 kV and digital images were captured with an ER-80 AMT 8 megapixel CCD camera.

Immunostaining

Leg samples were high pressure frozen as above, but were freeze substituted with a low temperature protocol utilizing Lowicryl HM20 resin (Polysciences #15924). Samples were freeze-substituted with fixing cocktail containing 0.2% uranyl acetate (in methanol), 0.2% glutaraldehyde in acetone with 5% water. We held the legs at −90 °C for 32 hrs, and then increased the temperature to −45 °C with a slope of 4 °C/hr. We gradually infiltrated the samples at −45 °C with a mixture of HM20 resin with acetone, 50% for 1.5 hrs, 75% for 1.5 hrs, 100% for 1.5 hrs, and finally overnight after a fresh exchange of 100% resin. Embedded samples were cured under UV light for 24 hrs at −45 °C, and then incubated for 24 hrs at room temperature before cutting.

We trimmed and oriented the resin blocks, and cut serial 0.5 μm longitudinal sections through the femoral leg segment and the femoral chordotonal organs. We treated the sections with 50 mM glycine for 10 min at room temperature and blocked the sections overnight at 4 °C in TBS (50 mM Tris-Cl,150 mM NaCl, pH 7.5) containing 10% BSA (Sigma). For staining with anti-TRPγ, we incubated the sections with primary rabbit TRPγ antibodies diluted 1:200 in TBS-T (50 mM Tris-Cl, 150 mM NaCl, 0.05% Tween-20, pH 7.5) for 72 hrs at 4 °C, washed with TBS, and incubated overnight in TBS-T at 4°C. For staining with α–CalX, we incubated the sections with primary rabbit CalX antibodies[41] diluted 1:200 in TBS-T overnight at 4 °C, washed with TBS, and incubated overnight in TBS-T at 4 °C. Sections probed with α–TRPγ and α–CalX were subsequently incubated in secondary antibodies [Alexa Fluor® 488 $F(ab')^2$ fragment of goat anti-rabbit IgG; A11070, Life technologies] diluted 1:500 in TBS for 1 hr at room temperature, washed with TBS, incubated overnight in TBS at 4 °C, and sealed under glass cover slips with Vectashield mounting media with DAPI. We viewed the sections using a Zeiss LSM700 and processed the images with Zen software (Carl Zeiss Microscopy).

Monitoring activities using actometers

We transferred individual 4 day-old male flies into recording tubes containing 1% agarose with 5% sucrose, and monitored locomotor activities using the Drosophila Activity Monitoring (DAM) system (Trikinetics Inc., Waltham, MA). We binned the number of activity events per individual fly every half-hour.

Negative geotaxis assay

We transferred 30 male flies (3–5 days old) to a 100 ml graduated cylinder, sharply tapped the cylinder down three times, and recorded videos (30 fps) of the flies ascending the sides of the cylinders. The climbing index is the percentage of flies that climbed past a line 10 cm from the bottom of the cylinder in 10 seconds.

Righting reflex assay

We introduced 30 male flies (3–5 days old) to a 100 ml graduated cylinder, and tapped the flies to the bottom as described for the negative geotaxis assay. We positioned a video

camera with a macro lens so that it could record the bottom surface of the cylinder (30 fps). After each set of taps, 0–5 flies fell on their backs and performed the righting reflex. Each group of 30 flies was tapped and recorded a maximum of 5 times. New groups of flies were then tested until the total number of observed righting reflexes was >100 per genotype. We analyzed the videos frame-by-fame to determine the elapsed time for completing the reflex.

Recording apparatus for analysis of locomotion behaviors

We recorded locomotion behavior at 200–250 frames per second (fps), and at a resolution of 1280 × 1024 pixels using a pco.1200s digital 10-bit CMOS camera system (PCO AG, Germany). A 3.3x macro zoom lens (NT56-524, Edmund Optics, Barrington, NJ) provided a 6.4 – 21.3 mm field of view on the 0.5″ sensor at a working distance of 90 mm. We mounted the camera orthogonally to a circular recording chamber (10 cm in diameter using optomechanical components from Thorlabs Inc.; Newton, NJ). The recording chamber was surrounded by 10 cm high white paper to reduce the influences of external visual stimuli, and was illuminated by an adjustable intensity array of 126 white LEDs behind a diffuser (CN-160 and CN-AC2, Amazon.com). The chamber accommodated a 34 mm × 10 mm × 4 mm walking platform (with or without a central gap) made of black Delrin® acetal resin. To obtain better contrast in the video recordings, we placed a pair of additional spotlights at both ends of the platform 10 cm away and 60° incident to the top surface. To prevent the flies from escaping, we surrounded the walking platform with 0.5 cm of water. To allow for precise positioning of the platform in the cameras field of view, we mounted the entire recording chamber on top of a 3-axis flexure stage (MBT616D, Thorlabs Inc., Newton, NJ).

Catwalk assay

We performed the assays using male flies with blinded genotypes. We cut the wings of the flies (3–5 days old) to ~1/4 their original length under ice anesthesia, and then recorded the flies walking behavior over a gapless platform at 250 fps. We collected three videos per fly, and 5 flies per genotype. Of the three recordings per fly, we chose the single video in which the fly exhibited the “straightest” crossing (no turns and/or stops as determined by slow motion analysis) for the tracking analysis. We tracked the frame-by-frame position of each leg tip using the MTrackJ plugin[57] in ImageJ[58].

Gap crossing assay

The gap crossing assay, which we performed using blinded genotypes, was similar to that described previously[12]. Briefly, we cut the wings of 3–5 day old male flies to ~1/4 their original length under ice anesthesia, and recorded their ability to cross gaps of various widths (1.0–4.0 mm) at 250 fps. We chose a 3.5 mm gap for the screening since this was a challenging but achievable width for wild-type. To screen for gap crossing proficiency (successful or unsuccessful), we recorded the first 10 crossing attempts for each fly. We tested 10 flies per genotype. The percentage of successful crossings represents the aggregate performance of 10 files in 100 total crossing attempts. During the screening, we recorded a small number of videos for each genotype to determine the body lengths.

To perform the detailed kinematic analyses during the gap crossings, we collected three videos for each fly, and recorded 5 flies per genotype. To perform the tracking analyses, we

chose a single video for each fly, based on the “straightest” crossing (orthogonal to the camera view as determined by slow motion analysis). We tracked the frame-by-frame position of each front leg tip, head position, and tail position using the MTrackJ plugin[57] for ImageJ[58].

Extracellular recordings

We performed electromyogram recordings of excitatory junction potentials from fly leg extensor muscles in response to tibia flexion as previously described[36, 37]. Briefly, we decapitated 3–5 day-old male flies under ice anesthesia, and allowed them to recover for 1 hour in a humidified chamber. If the flies were able to stand and walk, we mounted them for the recordings with their dorsal side up, and on the edge of a waxed cover slip so that the tibial segment of one leg was able to hang over the edge. The distal end of the femur was secured with wax. Tibia flexion was stimulated by sinusoidal displacement of a wire loop attached to the cone of a loudspeaker (273-092, RadioShack.com). A 2 Hz sine wave from a signal generator (Velleman PCGU1000, Allspectrum.com) resulted in ~20° of tibia movement about the femoral joint. We performed multiple sets of tibia flexion movements (10 movements/set), with each set spaced 1 minute apart to minimize habituation. We performed each recording with a 0.5–1 MΩ borosilicate electrode using an IE-210 intracellular electrometer (Warner Instruments LLC, Hamden, CT). Digital acquisition was performed using a PowerLab 4/30 DAQ with analysis in LabChart 5 (ADInstruments Inc., Colorado Springs, CO).

Cell culture

We cultured HEK293 cells (ATCC) in DMEM medium supplemented with 10% FBS and 1% penicillin/streptomycin at 37°C in a humidified atmosphere of 5% CO_2. Cells were plated onto glass coverslips coated with poly L-lysine for 24 hr before transfection. Split cells were co-transfected with plasmids encoding pcDNA3-TRPγ or empty pcDNA3.1 (mock) with GFP (1 μg and 0.5 μg, respectively) for 6–24 hr using either Polyfect or Lipofectamine LTX reagents (Qiagen, Valencia, CA or Life Technologies, Grand Island, NY).

Patch clamp recordings

We collected whole-cell current recordings of TRPγ in HEK293 cells under voltage-clamp conditions. Macroscopic TRPγ currents were evoked using voltage ramps or steps of 500 ms duration from −100 mV to 100 mV from a holding potential of −10 mV.

For hypoosmotic stimulation we used two different extracellular bath solutions: 1) an isotonic (300 mOsm) solution containing (in mM) 90 NaCl, 100 D-mannitol, 5 KCl, 2 $MgCl_2$, 2 $CaCl_2$, 10 HEPES, 10 D-glucose, pH 7.4 adjusted with NaOH; and 2) a hypotonic (210 mOsm) solution prepared by reducing the final concentration of D-mannitol to 10 mM without changing the ionic composition of the solution. The pipette solution was (in mM) 135 CsCl, 2 $MgCl_2$, 10 HEPES, 5 EGTA, 5 Na_2-ATP, pH 7.2 adjusted with CsOH.

Pressure stimulation was applied via a 100 ml syringe placed inline with a pressure manometer (SYS-PM100R, World Precision Instruments Inc., Sarasota, FL) connected to

the pressure port of the pipette microelectrode holder. Positive pressure steps of between +30 to +300 mmHg were applied from a resting pressure of −10 mmHg. Pressure was held constant during the recordings.

Macroscopic currents were acquired using an Axopatch 200B (Axon Instruments) patch clamp amplifier interfaced via a Digidata 1440A (Molecular Devices) to a PC running the pClamp 10.4 suite of software (Molecular Devices). Macroscopic currents were filtered at 1 kHz and digitized at 2 kHz. Whole cell capacitance and series resistances were routinely compensated. Only recordings where access resistance and capacitance changed <10% over the course of the experiment were used.

Supplementary Material

Refer to Web version on PubMed Central for supplementary material.

Acknowledgments

We thank the Johns Hopkins University School of Medicine Microscope Facility for assistance in preparing samples for automatic freeze substitution, immunostaining, and transmission election microscopy (RR026445). This work was supported by a grant to C.M. from the National Eye Institute (EY10852). B.A. was supported for a portion of this study by a postdoctoral fellowship from the National Institute of Neurological Disorders and Stroke (NS064684).

References

1. Biewener A, Daniel T. A moving topic: control and dynamics of animal locomotion. Biol Lett. 2010; 6:387–388. [PubMed: 20410030]
2. Dickinson MH, Farley CT, Full RJ, Koehl MA, Kram R, Lehman S. How animals move: an integrative view. Science. 2000; 288:100–106. [PubMed: 10753108]
3. Dietz V. Proprioception and locomotor disorders. Nat Rev Neurosci. 2002; 3:781–790. [PubMed: 12360322]
4. Windhorst U. Muscle proprioceptive feedback and spinal networks. Brain Res Bull. 2007; 73:155–202. [PubMed: 17562384]
5. Proske U, Gandevia SC. The proprioceptive senses: their roles in signaling body shape, body position and movement, and muscle force. Physiol Rev. 2012; 92:1651–1697. [PubMed: 23073629]
6. Dietz V. Gait disorders. Handb Clin Neurol. 2013; 110:133–143. [PubMed: 23312637]
7. Dietz V, Colombo G. Influence of body load on the gait pattern in Parkinson's disease. Mov Disord. 1998; 13:255–261. [PubMed: 9539338]
8. Konczak J, Krawczewski K, Tuite P, Maschke M. The perception of passive motion in Parkinson's disease. J Neurol. 2007; 254:655–663. [PubMed: 17420926]
9. Maschke M, Tuite PJ, Pickett K, Wächter T, Konczak J. The effect of subthalamic nucleus stimulation on kinaesthesia in Parkinson's disease. J Neurol Neurosurg Psychiatry. 2005; 76:569–571. [PubMed: 15774447]
10. Izawa J, Pekny SE, Marko MK, Haswell CC, Shadmehr R, Mostofsky SH. Motor learning relies on integrated sensory inputs in ADHD, but over-selectively on proprioception in autism spectrum conditions. Autism Res. 2012; 5:124–136. [PubMed: 22359275]
11. Mendes CS, Bartos I, Akay T, Marka S, Mann RS. Quantification of gait parameters in freely walking wild type and sensory deprived *Drosophila melanogaster*. Elife. 2013; 2:e00231. [PubMed: 23326642]
12. Pick S, Strauss R. Goal-driven behavioral adaptations in gap-climbing *Drosophila*. Curr Biol. 2005; 15:1473–1478. [PubMed: 16111941]

13. Strauss R, Heisenberg M. Coordination of legs during straight walking and turning in *Drosophila melanogaster*. J Comp Physiol A. 1990; 167:403–412. [PubMed: 2121965]
14. Li W, Feng Z, Sternberg PW, Xu XZ. A *C. elegans* stretch receptor neuron revealed by a mechanosensitive TRP channel homologue. Nature. 2006; 440:684–687. [PubMed: 16572173]
15. Tavernarakis N, Driscoll M. Degenerins. At the core of the metazoan mechanotransducer? Ann NY Acad Sci. 2001; 940:28–41. [PubMed: 11458685]
16. Venkatachalam K, Luo J, Montell C. Evolutionarily Conserved, Multitasking TRP Channels: Lessons from Worms and Flies. Handb Exp Pharmacol. 2014; 223:937–962. [PubMed: 24961975]
17. Cheng LE, Song W, Looger LL, Jan LY, Jan YN. The role of the TRP channel NompC in *Drosophila* larval and adult locomotion. Neuron. 2010; 67:373–380. [PubMed: 20696376]
18. Schafer WR. Mechanosensory molecules and circuits in *C. elegans*. Pflugers Arch. 2015; 467:39–48. [PubMed: 25053538]
19. Kernan MJ. Mechanotransduction and auditory transduction in *Drosophila*. Pflugers Arch. 2007; 454:703–720. [PubMed: 17436012]
20. Walker RG, Willingham AT, Zuker CS. A *Drosophila* mechanosensory transduction channel. Science. 2000; 287:2229–2234. [PubMed: 10744543]
21. Kernan M, Cowan D, Zuker C. Genetic dissection of mechanosensory transduction: mechanoreception-defective mutations of Drosophila. Neuron. 1994; 12:1195–1206. [PubMed: 8011334]
22. Gong Z, et al. Two interdependent TRPV channel subunits, Inactive and Nanchung, mediate hearing in *Drosophila*. J Neurosci. 2004; 24:9059–9066. [PubMed: 15483124]
23. Kim J, et al. A TRPV family ion channel required for hearing in *Drosophila*. Nature. 2003; 424:81–84. [PubMed: 12819662]
24. Homyk T, Sheppard DE. Behavioral mutants of *Drosophila melanogaster*. I. Isolation and mapping of mutations which decrease flight ability. Genetics. 1977; 87:95–104. [PubMed: 17248760]
25. Fowler MA, Montell C. *Drosophila* TRP channels and animal behavior. Life Sci. 2013; 92:394–403. [PubMed: 22877650]
26. Xu XZ, Chien F, Butler A, Salkoff L, Montell C. TRPγ, a *Drosophila* TRP-related subunit, forms a regulated cation channel with TRPL. Neuron. 2000; 26:647–657. [PubMed: 10896160]
27. Montell C, Rubin GM. Molecular characterization of the Drosophila *trp* locus: a putative integral membrane protein required for phototransduction. Neuron. 1989; 2:1313–1323. [PubMed: 2516726]
28. Gong WJ, Golic KG. Ends-out, or replacement, gene targeting in *Drosophila*. Proc Natl Acad Sci USA. 2003; 100:2556–2561. [PubMed: 12589026]
29. Zill S, Schmitz J, Büschges A. Load sensing and control of posture and locomotion. Arthropod Struct Dev. 2004; 33:273–286. [PubMed: 18089039]
30. Montell C. Physiology, phylogeny and functions of the TRP superfamily of cation channels. Science's STKE. 2001; 2001(90):re1.
31. Shanbhag SR, Singh K, Singh RN. Ultrastructure of the femoral chordotonal organs and their novel synaptic organization in the legs of *Drosophila melanogaster* Meigen (Diptera, Drosophilidae). Int J Insect Morphol Embryol. 1992; 21:311–322.
32. Chung YD, Zhu J, Han Y, Kernan MJ. *nompA* encodes a PNS-specific, ZP domain protein required to connect mechanosensory dendrites to sensory structures. Neuron. 2001; 29:415–428. [PubMed: 11239432]
33. Roy M, Sivan-Loukianova E, Eberl DF. Cell-type-specific roles of Na^+/K^+ ATPase subunits in *Drosophila* auditory mechanosensation. Proc Natl Acad Sci USA. 2013; 110:181–186. [PubMed: 23248276]
34. Rostaing P, Weimer RM, Jorgensen EM, Triller A, Bessereau JL. Preservation of immunoreactivity and fine structure of adult *C. elegans* tissues using high-pressure freezing. J Histochem Cytochem. 2004; 52:1–12. [PubMed: 14688212]
35. Burrows M. Parallel processing of proprioceptive signals by spiking local interneurons and motor neurons in the locust. J Neurosci. 1987; 7:1064–1080. [PubMed: 3572474]

36. Jin P, Griffith LC, Murphey RK. Presynaptic calcium/calmodulin-dependent protein kinase II regulates habituation of a simple reflex in adult *Drosophila*. J Neurosci. 1998; 18:8955–8964. [PubMed: 9787001]
37. Reddy S, Jin P, Trimarchi J, Caruccio P, Phillis R, Murphey RK. Mutant molecular motors disrupt neural circuits in *Drosophila*. J Neurobiol. 1997; 33:711–723. [PubMed: 9369146]
38. Trimarchi JR, Jin P, Murphey RK. Controlling the motor neuron. Int Rev Neurobiol. 1999; 43:241–264. [PubMed: 10218162]
39. Sun Y, Liu L, Ben-Shahar Y, Jacobs JS, Eberl DF, Welsh MJ. TRPA channels distinguish gravity sensing from hearing in Johnston's organ. Proc Natl Acad Sci USA. 2009; 106:13606–13611. [PubMed: 19666538]
40. Wang T, Jiao Y, Montell C. Dissecting independent channel and scaffolding roles of the *Drosophila* transient receptor potential channel. J Cell Biol. 2005; 171:685–694. [PubMed: 16301334]
41. Wang T, Xu H, Oberwinkler J, Gu Y, Hardie RC, Montell C. Light activation, adaptation, and cell survival functions of the Na^+/Ca^{2+} exchanger CalX. Neuron. 2005; 45:367–378. [PubMed: 15694324]
42. Sukharev S, Sachs F. Molecular force transduction by ion channels: diversity and unifying principles. J Cell Sci. 2012; 125:3075–3083. [PubMed: 22797911]
43. Jörs S, Kazanski V, Foik A, Krautwurst D, Harteneck C. Receptor-induced Activation of *Drosophila* TRPγ by Polyunsaturated Fatty Acids. J Biol Chem. 2006; 281:29693–29702. [PubMed: 16901908]
44. Hamill OP, McBride DW Jr. Induced membrane hypo/hyper-mechanosensitivity: A limitation of patch-clamp recording. Annu Rev Physiol. 1997; 59:621–631. [PubMed: 9074780]
45. Rakel, RE. Chapter 23: Growth and Development. In: Kimmel, SR.; Ratliff-Schaub, K., editors. Textbook of Family Medicine. 8. Elsevier/Saunders; 2011.
46. Lee J, Moon S, Cha Y, Chung YD. *Drosophila* TRPN(=NOMPC) channel localizes to the distal end of mechanosensory cilia. PLoS One. 2010; 5:e11012. [PubMed: 20543979]
47. Hamilton ES, Schlegel AM, Haswell ES. United in Diversity: Mechanosensitive Ion Channels in Plants. Annu Rev Plant Biol. 2014
48. Maathuis FJ. Vacuolar two-pore K^+ channels act as vacuolar osmosensors. New Phytol. 2011; 191:84–91. [PubMed: 21371040]
49. Plant TD. TRPs in mechanosensing and volume regulation. Handb Exp Pharmacol. 2014; 223:743–766. [PubMed: 24961968]
50. Moon SJ, Lee Y, Jiao Y, Montell C. A *Drosophila* gustatory receptor essential for aversive taste and inhibiting male-to-male courtship. Curr Biol. 2009; 19:1623–1627. [PubMed: 19765987]
51. Brand AH, Perrimon N. Targeted gene expression as a means of altering cell fates and generating dominant phenotypes. Development. 1993; 118:401–415. [PubMed: 8223268]
52. Venken KJ, et al. Versatile P[acman] BAC libraries for transgenesis studies in *Drosophila melanogaster*. Nat Methods. 2009; 6:431–434. [PubMed: 19465919]
53. Venken KJ, He Y, Hoskins RA, Bellen HJ. P[acman]: a BAC transgenic platform for targeted insertion of large DNA fragments in *D. melanogaster*. Science. 2006; 314:1747–1751. [PubMed: 17138868]
54. McDonald K, Morphew MK. Improved preservation of ultrastructure in difficult-to-fix organisms by high pressure freezing and freeze substitution: I. *Drosophila melanogaster* and *Strongylocentrotus purpuratus* embryos. Microsc Res Tech. 1993; 24:465–473. [PubMed: 8490232]
55. Walther P, Ziegler A. Freeze substitution of high-pressure frozen samples: the visibility of biological membranes is improved when the substitution medium contains water. J Microsc. 2002; 208:3–10. [PubMed: 12366592]
56. McDonald KL, Morphew M, Verkade P, Müller-Reichert T. Recent advances in high-pressure freezing: equipment- and specimen-loading methods. Methods Mol Biol. 2007; 369:143–173. [PubMed: 17656750]
57. Meijering E, Dzyubachyk O, Smal I. Methods for cell and particle tracking. Methods Enzymol. 2012; 504:183–200. [PubMed: 22264535]

58. Schneider CA, Rasband WS, Eliceiri KW. NIH Image to ImageJ: 25 years of image analysis. Nat Methods. 2012; 9:671–675. [PubMed: 22930834]

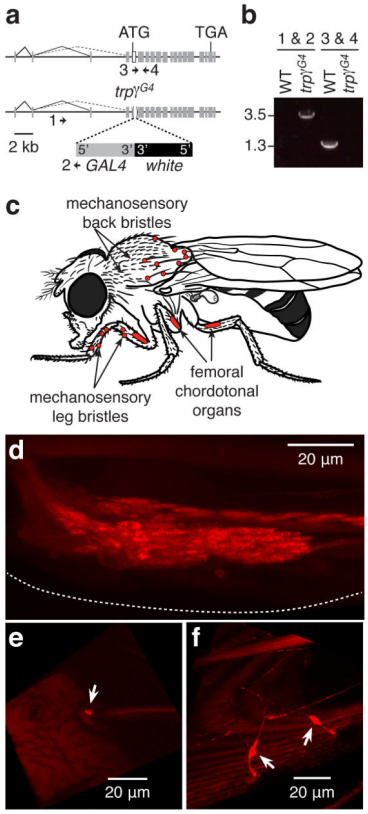

Figure 1. Expression of the *trpγ* reporter in mechanosensitive and proprioceptive organs

(a) Schematic of the *trpγ* gene and *trpγ*^{G4} knockout generated by ends-out homologous recombination[28].

(b) PCR amplification of genomic DNA to identify flies with the *trpγ*^{G4} mutation. The positions of the primer pairs that were used are indicated in panel (a). The upper and lower tick marks to the left represent the positions of the 3.5 and 1.3 kb markers.

(c) Cartoon depicting the location of mechanosensitive sensilla and proprioceptive organs distributed on the fly. Sites of prominent *trpγ* reporter expression are labeled in red.

(d–f) Expression of the *trpγ*^{G4} reporter (*trpγ*^{G4}/+;*UAS-dsRed).* Scale bars 20 μm.

(d) Femoral chordotonal organ in a foreleg.

(e) White arrow indicates neuron innervating a macrochaete in the dorsal thorax.

(f) White arrows indicate neurons innervating large mechanosensory bristles of the femoral segment of the foreleg.

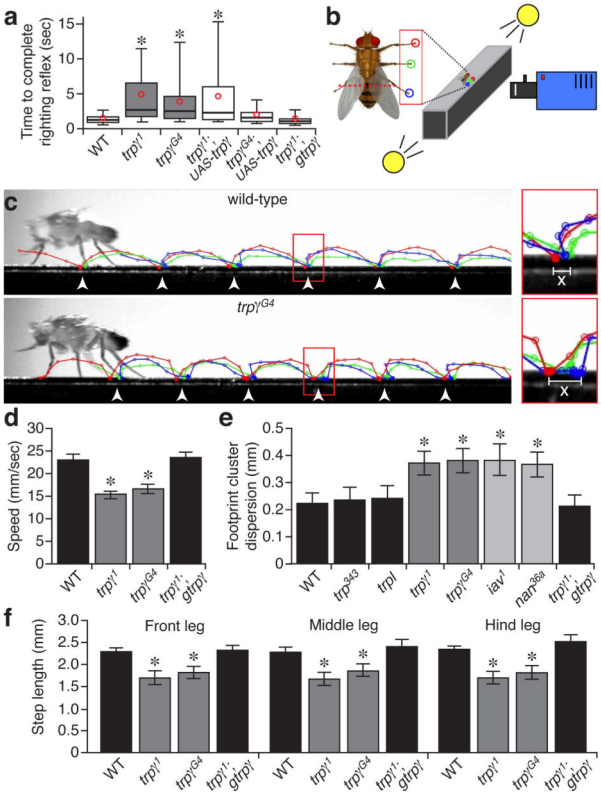

Figure 2. Comparison of wild-type and *trpγ* righting reflex and leg coordination during walking

(a) Quantification of the righting reflex. In each box plot the solid black bar represents the median value and open red circle the mean. The boxes denote the 25% and 75% quantiles of the distribution. The whiskers represent 5% and 95% quantiles. Wild-type, WT. Non-parametric Mann-Whitney U test, n≥100. *$p \leq 0.05$.

(b) Schematic of the catwalk behavioral setup. To track the movements of the leg tips on one side of the body, we positioned a high-resolution, high-frame rate camera orthogonally at the level of the catwalk: front (red), middle (green), and hind (blue). The wings were clipped (red dashed line) to prevent the animal from flying. We recorded at 250 fps.

(c) Representative crossings of wild-type and $trp\gamma^{G4}$ flies showing footprint clustering on the catwalk. Footprint cluster dispersions (X, red inset boxes enlarged in right panel) were measured as the width of each cluster using the initial contact point on the platform for each leg.

(d) Average walking speed of flies across the catwalk.

(e) Footprint cluster dispersion during walking.

(f) Quantification of step length for the front, middle, and hind legs during walking.

Mean ±SEM, n≥5. ANOVA with Dunnet's *post-hoc* analysis. *$p \leq 0.05$.

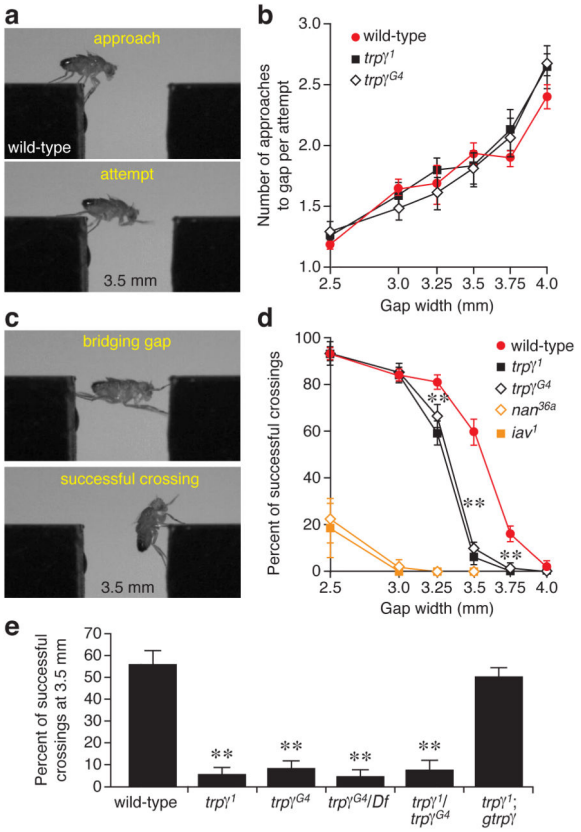

Figure 3. Assaying wild-type and *trpγ* gap crossing at various gap widths

We recorded videos at 250 fps.

(a) Still frames from the video showing a male wild-type fly during a gap crossing at 3.5 mm. We defined the approach posture (upper panel) as a pause at the gap with three legs on the starting wall. We defined an attempt (lower panel), as repeated leg-over-head (LOH) motion/stroke towards the opposite side of the gap.

(b) Number of approaches/attempt at crossing, as a function of the gap width.

(c) Still frames from a video showing a wild-type male fly successfully crossing a 3.5 mm gap. The fly bridged the gap with its front and hind legs (upper panel). After gripping the opposite side with its front legs, the fly released its hind legs, which allowed its body to swing across the gap (lower panel).

(d) Percent of successful crossings. The percentages were based on 10 attempts per fly at different gap widths. ANOVA with Dunnet's *post-hoc* analysis, n≥10, $^{**}p \leq 0.01$.

(e) Quantification of gap crossing success at 3.5 mm for the animals with the indicated genotypes. ANOVA with Dunnet's *post-hoc* analysis. n≥10, $^{**}p \leq 0.01$.

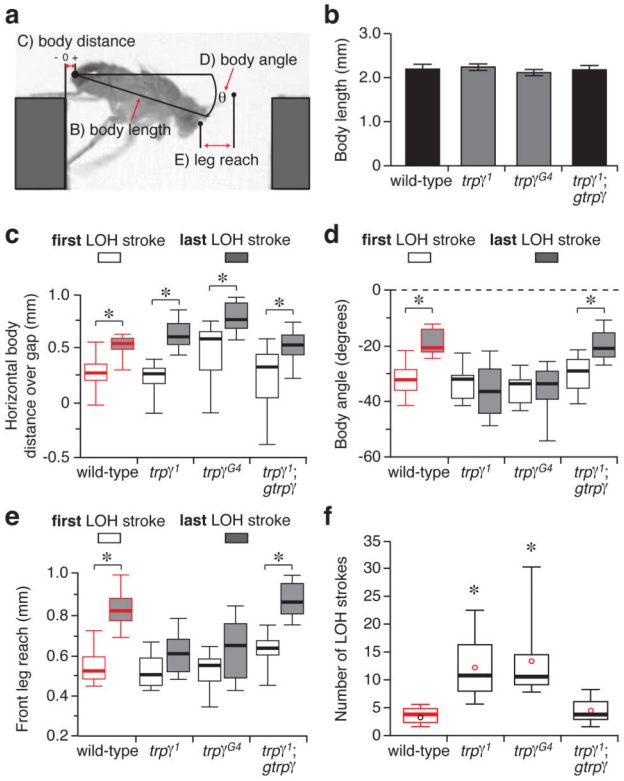

Figure 4. Abilities of *trpγ* mutants to make the fine postural adaptions necessary to fully extend their reach during gap crossing

(a) Illustration of the different postural metrics extracted from gap crossing videos recorded at 200 fps.

(b) Quantification of body lengths. Mean ±SEM, n≥10. Lack of statistical significance was determined by ANOVA.

(c) Quantification of the changes in horizontal body position over the gap from the first LOH stoke (open boxes) to the last LOH stroke (grey filled boxes).

(d) Quantification of the changes in body angle towards horizontal from first LOH to last LOH.

(e) Quantification of the changes in front leg reach from first LOH to last LOH.

(f) Quantification of the total number of LOH strokes performed by each fly during a crossing attempt.

For each box plot in panels (c–f) the solid bar represents the median value, the box denotes the 25% and 75% quantiles of the distribution, and the whiskers represent 5% and 95% quantiles. For panels (c–e) statistical significances were determined by non-parametric Wilcoxon signed-rank tests, n≥10, *$p \leq 0.05$. For panel F statistical significances were determined by non-parametric Mann-Whitney U tests. n≥10, *$p \leq 0.05$.

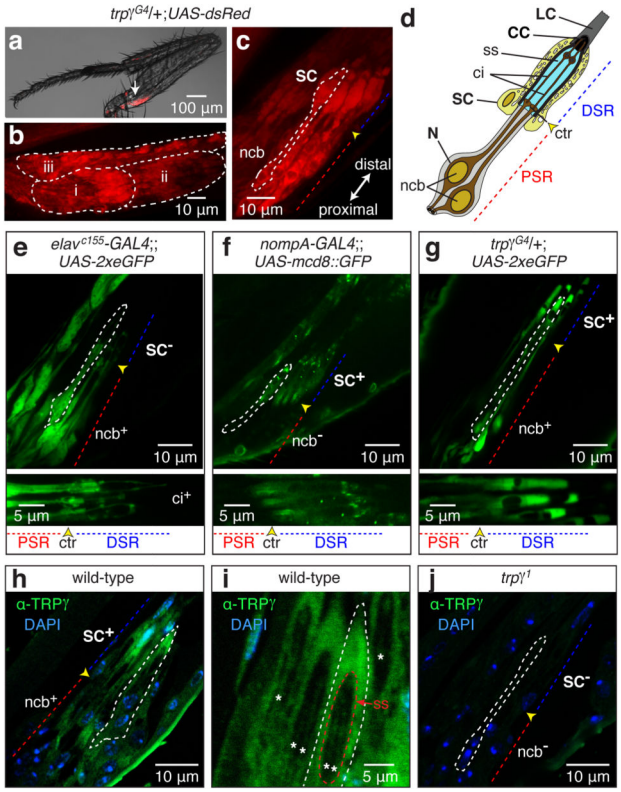

Figure 5. TRPγ localizes to the neurons and scolopale cells of the femoral chordotonal organs

(a) The *trpγ*^{G4} reporter drove *UAS-dsRed* expression in the FCO of the forelegs (white arrow). Scale bar 100 µm.

(b) *trpγ*^{G4} staining of the three bundles/groups of aligned scolopidia, i, ii, and iii that comprise the FCO (dashed lines). Scale bar 10 µm.

(c) Reconstruction of *trpγ*^{G4} FCO staining revealing the structure of multiple, aligned scolopidia. Neuronal cell bodies (ncb) and scolopale cells (SC) are situated in the proximal scolopidial region (PSR) and the distal scolopidial region (DSR), respectively. Scale bar 10 µm.

(d) Schematic of an individual scolopidia showing the neurons (N), neuron cell bodies (ncb), cilia (ci), cap cell (CC), ligament cell (LC), scolopale cell (SC), and scolopale space (ss). Ciliary transition root (ctr, yellow arrow) demarcates the PSR (red dashed line) and DSR (blue dashed line).

(e–j) Staining of FCO scolopidia bundles. White dashed line outlines single scolopidia units. Scale bars 5 µm.

(e) Pan-neuronal *elav*^{c155}*-Gal4* staining revealed fluorescence in the neuron cell bodies (ncb^{+}) and in the scolopale cell layer, but not in the scolopale cells (SC^{-}). Staining of thin-paired cilia (ci^{+}) was seen in the DSR. The distal ends of the scolopidia are enlarged for detail (bottom panel).

(f) Scolopale cell specific *nompA-Gal4* staining revealed fluorescence only in the scolopale cells (SC^{+}) not in the neuron cell bodies (ncb^{-}). Neither axonal nor ciliary signal was detected using *nompA-Gal4* (bottom panel).

(g) The *trpγ*^{G4} reporter stained both neuronal cell bodies (ncb^{+}) and scolopale cells (SC^{+}). Staining of the scolopale cells obscured the sensory cilia (bottom panel).
(h) Longitudinal section of wild-type FCO immunostained with α–TRPγ and counterstained with DAPI. Antibodies strongly labeled the distal ends of the scolopale cells (SC^{+}), and more diffusely labeled neuron cell bodies (ncb^{+}).
(i) Enlarged view of the DSR showing multiple scolopale spaces (ss, red dashed line). Within the ss, α–TRPγ stained cilia, but labeling of such thin processes was weak (white asterisks, at the proximal end of each cilia).
(j) Longitudinal section of *trpγ*^{1} FCO immunostained with α–TRPγ and counterstained with DAPI.

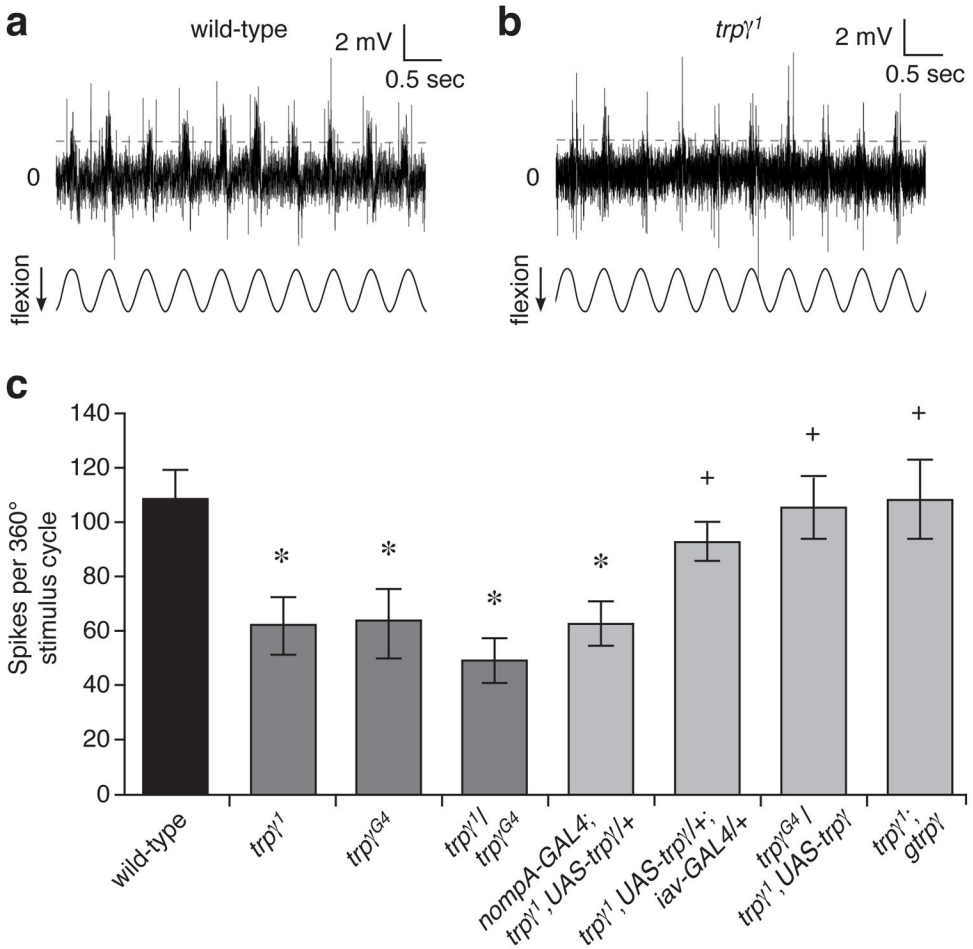

Figure 6. Assaying tibial extensor muscle activity by electromyogram (EMG) recordings

(a) Representative EMG recordings of tibial extensor muscle activity in response to tibial flexion at 2 Hz. The grey dashed line represents a spike detector threshold 10% above the 1 sec mean noise prior to stimulation.

(b) Quantification of the change the number of spikes elicited per 360° of flexion for flies of different genotypes. Mean ±SEM, n≥5. ANOVA with Dunnet's *post-hoc* analysis. *$p \leq 0.05$ with wild-type as control group. $^{+}p \leq 0.05$ with *trp*γ^{1} as the control group.

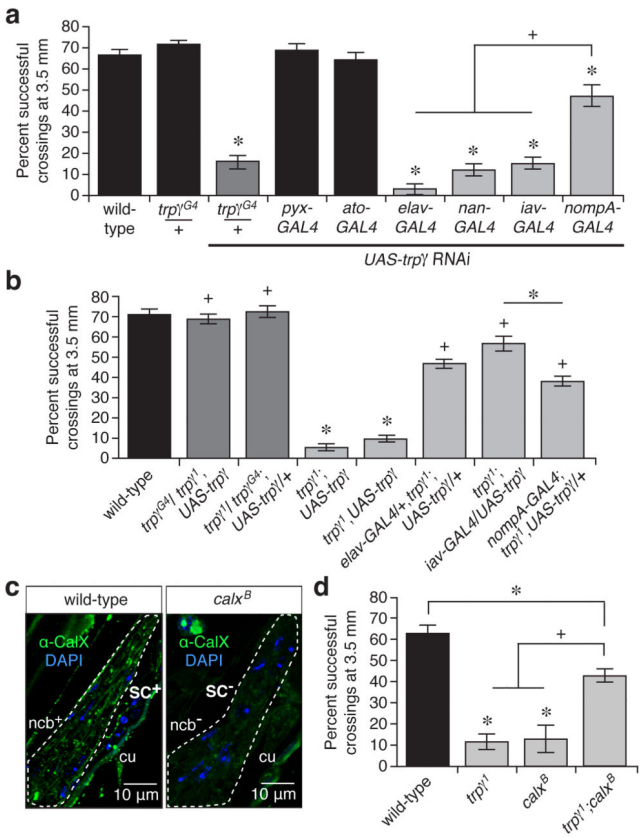

Figure 7. TRPγ dependent Ca^{2+} influx is required in neurons and scolopale cells for effective gap crossing

(a) Percentage of animals that were successful at crossing a 3.5 mm gap after knocking down *trpγ* (*UAS-trpγ* RNAi) with the indicated *GAL4* drivers. Mean ±SEM, n≥30. ANOVA with Dunnet's *post-hoc* analysis. *$p \leq 0.05$ with wild-type as the control group.

(b) Gap crossing success (3.5 mm gap) of $trp\gamma^1$ flies that expressed *UAS-trpγ* under the control of a variety of *Gal4* drivers. Data are presented as mean ±SEM, n≥30. ANOVA with Dunnet's *post-hoc* analysis. *$p \leq 0.05$ with wild-type as the control group. $^{+}p \leq 0.05$ with *UAS-trpγ* on the 2nd or 3rd chromosome in a $trp\gamma^1$ mutant background as the control group.

(c) Longitudinal section through a wild-type and $calx^B$ FCO immunostained with α–CalX and counterstained with DAPI. The antibodies labeled the scolopale cells (SC^+), and neuron cell bodies (ncb^+) in wild-type sections only. Non-specific staining of the cuticle (cu) was observed in both wild-type and mutant sections. Scale bars 10 μm.

(d) Gap crossing success (3.5 mm gap) of $trp\gamma^1$, $calx^B$, and the $trp\gamma^1$;$calx^B$ double mutant. Data are presented as mean ±SEM, n≥10. ANOVA with Tukey's *post-hoc* analysis. *$p \leq 0.05$.

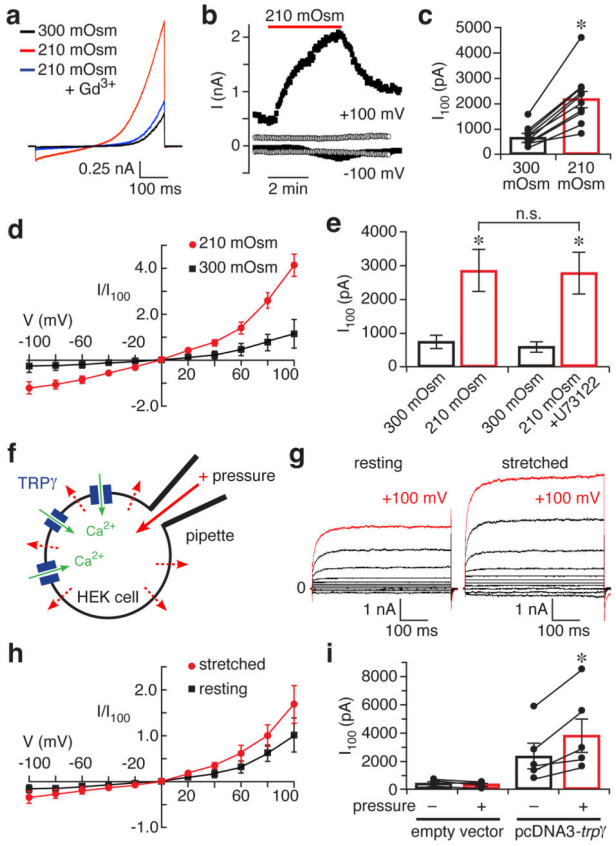

Figure 8. TRPγ is activated by membrane stretch *in vitro*

(a) Overlay of current traces showing the effects of hypoosmotic solution and 100 μm Gd^{3+} on recombinant TRPγ in HEK cells. Current was evoked with a voltage ramp from −100 to 100 mV from a holding potential of −10 mV.

(b) Time course of hypoosmotic stimulus on TRPγ currents. Outward and inward macroscopic currents were measured at +100 and −100 mV, respectively, in representative transfected (black squares) and untransfected (open circles) HEK cells.

(c) Graph of paired current measurements showing the effects of hypoosmotic stimulus on macroscopic TRPγ currents in HEK cells. Data bars are presented as mean ±SEM, n=10. Paired two-tailed *t*-test, *$p \leq 0.05$.

(d) Current-voltage (I–V) curves for HEK cells expressing recombinant TRPγ in isotonic (black squares) and hypotonic (red circles) solutions. Data are presented as mean ±SEM, n=10.

(e) Summary graph showing the effect of hypoosmotic solution on TRPγ currents in the presence and absence of a PLC inhibitor U73122 (5 uM). Data bars are presented as mean ±SEM, n=10. Paired two-tailed *t*-test, *$p \leq 0.05$.

(f) Cartoon depicting the activation of TRPγ by membrane stretch induced by positive pipette pressure in a whole cell configuration.

(g) Overlay of current traces showing the effects of pressure-induced membrane stretch on the activities of TRPγ recorded from the same HEK cell. Current was evoked with voltage steps from −100 to 100 mV from a holding potential of −60 mV.

(h) I–V curves for HEK cells expressing recombinant TRPγ under resting (black squares) and stretched (red circles) conditions. Data are presented as mean ±SEM, n=5.
(i) Graph of paired current measurements showing the effects of pressure-induced membrane stretch on macroscopic currents recorded from HEK cells transfected with either pcDNA3-*trpγ* or an empty vector. Data bars are presented as mean ±SEM, n=5. Paired two-tailed *t*-test, *$p \leq 0.05$.